Atmos. Chem. Phys. Discuss., 11, 19179–19212, 2011
www.atmos-chem-phys-discuss.net/11/19179/2011/
doi:10.5194/acpd-11-19179-2011

Atmospheric Chemistry and Physics Discussions

Estimation of NO_x emissions from Delhi using car MAX-DOAS observations and comparison with OMI satellite data

R. Shaiganfar[1], S. Beirle[1], M. Sharma[2], A. Chauhan[2], R. P. Singh[2,3], and T. Wagner[1]

[1]Max-Planck-Institute for Chemistry, Mainz, Germany
[2]Research and Technology Development Centre, Sharda University, Greater Noida, India
[3]School of Earth and Environmental Sciences, Schmid College of Science, Chapman University, Orange 92866, USA

Received: 20 April 2011 – Accepted: 30 June 2011 – Published: 5 July 2011

Correspondence to: R. Shaiganfar (r.shaiganfar@mpic.de)

Published by Copernicus Publications on behalf of the European Geosciences Union.

Abstract

We present the first Multi-Axis- (MAX-) DOAS observations in India performed during April 2010 and January 2011 in Delhi and nearby regions. The MAX-DOAS instrument was mounted on a car roof, which allowed us to perform measurements along individual driving routes. From car MAX-DOAS observations along closed circles around Delhi, together with information on wind speed and direction, the NO_x emissions from the greater Delhi area were determined: our estimate of 3.7×10^{25} molec s^{-1} is found to be slightly lower than the corresponding emission estimates using the EDGAR data base and substantially smaller compared to a recent study by Gurjar et al. (2004). We have also used the MAX-DOAS observations of the tropospheric NO_2 VCD for validation of simultaneous satellite observations from the OMI instrument and found a good agreement of the spatial patterns. The absolute values show a reasonably good agreement. However, OMI data tends to underestimate the tropospheric NO_2 VCDs in regions with high pollution levels, and tends to overestimate the tropospheric NO_2 VCDs in more clean areas. These findings indicate possible discrepancies between the true vertical NO_2 profiles and the profile assumptions in the OMI satellite retrieval.

1 Introduction

Delhi, home of 19 million people, second largest metropolitan city (http://www.indiaonlinepages.com/population/delhi-population.html) is located in the Indo-Gangetic plains in India. The growing population and human activities increase the atmospheric pollution which is e.g. the cause of the dense fog, smog and haze during winter season (December and January) every year (Singh et al. 2004, 2005; Ramanathan and Ramana, 2005; Ramanathan et al., 2005; Gautam et al. 2007). In the years 2005 and 2006, about 4.8 Million vehicles were in operation in Delhi.

ACPD
11, 19179–19212, 2011

In the last three decades the atmospheric trace gas and aerosol loading has increased in the Indo-Gangetic plains due to intense urbanization, anthropogenic activities, industrial growth and energy demand. Especially in the northern part of India, the pollutants swing in the Indo-Gangetic basin depending upon the meteorological conditions. The sources of atmospheric pollutants are localized and heterogeneous and depended on season (Gurjar et al., 2004; Goyal et al., 2006; Lal, 2007).

The measurements of atmospheric pollutants are not only important for air quality, but also to understand the radiative forcing and its impact on climate (Ravishankara et al., 2004; Seinfeld and Pandis, 2006). Currently, still large uncertainties exist with respect to the total emissions of pollutants and their impact on local, regional, and possibly also global scale. The corresponding uncertainties are especially large for many Megacities.

In this study, we present top-down emission estimates for nitrogen oxides ($NO_x = NO + NO_2$) for Delhi from car MAX-DOAS observations. Nitrogen oxides are formed in combustion processes (e.g. from vehicles, and power plants); they are toxic (Elsayed, 1994; World Health Organization, 2003) and also involved in important photochemical processes. Together with the emissions of volatile organic compounds, they control tropospheric ozone chemistry and oxidising capacity (Jacob, 1999; Seinfeld and Pandis, 2006).

We use Multi-Axis-Differential Optical Absorption Spectroscopy (MAX-DOAS) measurements (Hönninger et al., 2002; Van Roozendael et al., 2004; Wittrock et al., 2004; Wagner et al., 2004; Brinksma et al., 2008 and references therein) to quantify the NO_x emissions of Delhi. The MAX-DOAS instrument was mounted on a car roof, and continuous measurements were performed on closed driving routes around the city center on three days during April 2010 and one day in January 2011. In combination with wind data, the total emissions from the encircled area can be determined (Johansson et al., 2008, 2009; Rivera et al., 2009; Ibrahim et al., 2010; Wagner et al., 2010).

In addition to the quantification of the NO_x emissions, the MAX-DOAS results are also used for the validation of satellite observations of the tropospheric NO_2 VCD. Car

ACPD
11, 19179–19212, 2011

MAX-DOAS observations yield valuable information about the horizontal heterogeneity of the NO_2 distribution, which can not be resolved by the satellite observations, making them superior to validation with MAX-DOAS measurements at fixed locations.

The paper is organized as follows: in Sect. 2, we give details of the instrument, the measurement campaign and the retrieval of the tropospheric NO_2 VCD. Section 3 presents the determination of the NO_x emissions of Delhi and comparison with the EDGAR emission inventory. In Sect. 4, the MAX-DOAS tropospheric NO_2 VCDs are compared to simultaneous satellite observations from the Ozone Monitoring Instrument (OMI).

2 2 MAX-DOAS observations and data analysis

2.1 Car MAX-DOAS instrument

The Mini-MAX-DOAS instrument is a fully automated, light weighted spectrometer (13 cm × 19 cm × 14 cm) designed for the spectral analysis of scattered sunlight (Bobrowski et al., 2003). It consists of a sealed aluminium box containing the entrance optics, a fibre coupled spectrograph and the controlling electronics. A stepper motor mounted outside the box rotates the whole instrument to control the elevation of the viewing angle (angle between the horizontal and the viewing direction). The entrance optics consists of a quartz lens of focal length $f = 40$ mm coupled to a quartz fibre bundle which leads the collected light into the spectrograph (field of view is $\sim 1.2^{\circ}$). The light is dispersed by a crossed Czerny-Turner spectrometer (USB2000+, Ocean Optics Inc.) with a spectral resolution of 0.7 nm over a spectral range from 320–460 nm. A one-dimensional CCD (Sony ILX511, 2048 individual pixels) is used as detector. The measurements were controlled from a laptop using the DOASIS software (Kraus, 2004).

ACPD
11, 19179–19212, 2011

2.2 Overview on measurements around Delhi

For the mobile observations measurements around Delhi, the Mini-MAX-DOAS instrument was mounted on the roof top of a car with the telescope pointing parallel to the driving direction, pointing backward (April 2010)/forward (January 2011). The measurements started from Greater Noida to Delhi and around Delhi; the routes are shown in Fig. 1 for all the four days (13, 14, and 15 April 2010 and 15 January 2011).

The sequence of elevation angles was chosen to: $1 \times 90^{\circ}$, $5 \times 22^{\circ}$, $1 \times 45^{\circ}$, $5 \times 22^{\circ}$ and the duration of an individual measurement was about 60 s. For the measurements on 15 January 2011, an elevation angle of 30° was set up instead of 22° during April 2010. The temperature setpoint of the mini MAX-DOAS was 15 °C in April and 5 °C in January. A handy GPS was used to track the coordinates of the route along which the observations were made.

All the three days in April 2010 were cloud-free, the aerosol optical depth derived from MODIS satellite was found in the range of 0.2–0.5 at 550 nm. The wind direction was mostly north-westerly, and the temperature was found in the range 35–45 °C. On 15 January 2011, the AOD was found to be only 0.1 in the afternoon. During the start of the measurements at 11 a.m. the AOD may be higher, but we do not have any estimate due to non availability of MODIS aerosol data. The wind is found to be westerly and temperature to vary in the range 15–20 °C. The time to complete one full circle around the route (Fig. 1) took about 3 to 5 h.

In contrast to MAX-DOAS observations at fixed locations, during car MAX-DOAS observations we have used rather high elevation angles to avoid shades from nearby obstacles (e.g. buildings or trees). We took observations at elevation angles of 22° (April 2010) and 30° (January 2011). From such high elevation angles usually no profile information can be retrieved, but we can obtain the total tropospheric trace gas column density. Measurements at high elevation angles are less affected by aerosols than observations at more low elevation angles.

ACPD
11, 19179–19212, 2011

2.3 Spectral analysis

The measured spectra are analysed using the DOAS method (Platt and Stutz, 2008). A wavelength range 435–456 nm was selected for the analysis. Several trace gas absorption cross sections (NO_2 at 298 K (Vandaele et al., 1996), H_2O at 298 K (Rothman et al., 2005), Glyoxal at 296 K (Volkamer et al., 2005), O_3 at 243 K (Bogumil et al., 2003), O_4 at 296 K (Hermans et al., 1999)), as well as a Fraunhofer reference spectrum, a Ring spectrum (calculated from the Fraunhofer spectrum) and a polynomial of third order were included in the spectral fitting process, using the WinDOAS software (Fayt and van Roozendael, 2001).

The wavelength calibration was performed based on a high resolution solar spectrum (Kurucz et al., 1984). The output of the spectral analysis is the slant column density (SCD), the integrated trace gas concentration along the light path through the atmosphere. From the spectral analysis, also the uncertainty of the retrieved SCD is determined; for the NO_2 analysis it is typically <15 %.

Since a measured spectrum is used as Fraunhofer reference, the retrieval result represents the difference of the SCDs of the measurement at low elevation angle α and the Fraunhofer reference spectrum taken at 90° elevation, the so called differential SCD or DSCD:

$$\mathrm{DSCD}_\alpha = \mathrm{SCD}_\alpha - \mathrm{SCD}_{\mathrm{Fraunhofer}} \quad (1)$$

A typical fit result is shown in Fig. 2.

We have considered elevation angles (α) of 22° for measurements during April 2010 and of 30° during January 2011. We considered DSCD_αs with RMS of residuals smaller than 2.5×10^{-3}.

2.4 Estimation of the tropospheric VCD

To determine the SCD_α of a measurement, the $\mathrm{SCD}_{\mathrm{Fraunhofer}}$ has to be added as discussed earlier by Wagner et al. (2010) and Ibrahim et al. (2010). The $\mathrm{VCD}_{\mathrm{trop}}$ is

ACPD
11, 19179–19212, 2011

obtained from the SCD_α by dividing by the air mass factor (AMF):

$$VCD_{trop} = SCD_\alpha / AMF_\alpha \quad (2)$$

For many applications, the AMF is retrieved from radiative transfer simulations (Solomon et al., 1987), but here the so called geometric approximation (Brinksma et al., 2008, Andreas Richter, personal communication 2006) is used:

$$AMF(\alpha) = 1/\sin(\alpha) \quad (3)$$

Using Eq. (3), the tropospheric AMF were found to be 2.67 and 2 for elevation angles of 22° and 30°, respectively. Depending on the aerosol load, cloud condition and vertical trace gas profile, the true AMF can show substantial deviations from the geometric approximation. However, NO_2 is generally located near the surface; therefore the deviations for our measurements are expected to be small (see next section).

2.5 Effect of aerosols on the measurements

The geometric approximation for tropsopheric AMF (Eq. 3) is only valid if the light path through the trace gas layer of interest can be well approximated by a simple geometric path. This assumption is usually fulfilled for shallow trace gas layers and low aerosol loads, since the observed light is typically scattered from above the trace gas layer. But in the presence of high aerosol extinction, a substantial fraction of the observed light might be scattered from inside the trace gas layer and the geometric approximation is not appropriate for the complete trace gas layer.

Depending on the elevation angle and the amount and properties of the aerosols, scattering inside the trace gas layer may either increase (for high elevation angles) or decrease (for lower elevation angles) the true AMF compared to the geometric approximation (Wagner et al., 2004). Thus, the true tropospheric trace gas VCD will be either over- or underestimated.

We have quantified these deviations from the geometric approximation using the Monte Carlo radiative transfer model McARTIM (Deutschmann et al., 2011) for various

ACPD
11, 19179–19212, 2011

aerosol scenarios and NO_2 layer heights. For NO_2 layer heights ≤500 m and for moderate aerosol optical depth (about <1), the deviations from the geometric approximation are found to be below 20 % (see results for elevation angle of 22° in Fig. 3). Such low NO_2 layer heights were found over polluted places (Milano, Italy, Wagner et al., 2011). For measurements at an elevation angle of 30° (15 January 2011) similar results are found (not shown).

The error in the spectral retrieval is of the order of 15 % (see Sect. 2.3). Thus, we estimate the total error in the estimation of retrieved tropospheric NO_2 VCD to be about 25 %.

3 3 Estimation of NO_x emissions

3.1 Emissions from the encircled area

The total NO_2 emissions from the encircled area are determined from the following equation (Ibrahim et al., 2010):

$$F_{NO_2} = \oint_S VCD_{NO_2}(s) \times \boldsymbol{w} \times \boldsymbol{n} \times ds \tag{4}$$

Here $\boldsymbol{n}(s)$ indicates the normal vector parallel to the Earth's surface and orthogonal to the driving direction at the position s of the driving route; $\boldsymbol{w}$ is the average wind vector within the trace gas layer. The integral of Eq. (4) is evaluated for the MAX-DOAS measurements around Delhi. Because of the finite integration time of individual spectra, the integral is approximated by a sum of the individual polygonal lines.

$$\begin{aligned} F_{NO_2} &= \sum_i VCD_{NO_2}(s_i) \times \boldsymbol{w} \times \boldsymbol{n} \times \Delta s_i \\ &= \sum_i VCD_{NO_2}(s_i) \times \boldsymbol{w} \times \sin(\beta_i) \times \Delta s_i \end{aligned} \tag{5}$$

ACPD
11, 19179–19212, 2011

The location, length and direction of each segment is taken from GPS data, which were stored at each second using a GPS-Logger (HOLUX, m.247). The distance between two measurements Δs_i is taken as the geometric difference between the locations at the beginning of two successive measurements. From the same segment, the angle β_i between the driving route and the wind direction is calculated.

Wind fields are taken from analyses of the European Centre for Medium-Range Weather Forecasts (ECMWF, full scientific and technical documentations are found from the website http://www.ecmwf.int/research/ifsdocs/CY33r1/index.html). Since we are interested in quantifying local emissions, we consider the average of the 3 lowermost layers (about 0, 30 and 60 m above ground), linearly interpolated in time for the average MAX-DOAS time.

We estimate the uncertainty of the flux estimation due to the choice of wind fields by (a) considering the 3 vertical layers separately (causing variations within 15 %), and (b) taking the closest ECMWF output times at 06:00 and 12:00 UTC instead of interpolating (causing variations within 10 % except for 15 January, where the wind fields at 12:00 UTC have changed significantly, whereas the measurements were taken close to 06:00 UTC). Overall, we estimate the error due to wind fields as 18 %.

The measured NO_2 VCDs together with the wind fields for the four measurement days are shown in Fig. 4. In general, the highest values of NO_2 VCDs are found at the lee side of the city, as expected.

On some days, due to instrument problems, gaps along the driving route occurred; this was mainly due to disturbances caused by uneven road conditions. Due to such problems, NO_2 data are missing at some locations, which has contributed to the larger uncertainties in the estimation of the total emissions. We estimate these uncertainties in a simple way: in a first calculation, we determine the total emissions clockwise, in a second calculation counter-clockwise. In both cases, the NO_2 VCD from the last measurements at the beginning of the gap is considered as the true value for the whole gap. From both calculations, we determine the average emissions and the corresponding uncertainties.

ACPD
11, 19179–19212, 2011

In the next step, correction factors accounting for the partitioning between NO and NO_2 (c_L) and for the finite lifetime of NO_x (c_τ) are applied (see Ibrahim et al., 2010) to derive the complete NO_x emissions from the encircled areas:

$$F_{NO_x} = c_L \times c_\tau \times F_{NO_2} \quad (6)$$

Here c_L is simply the ratio of NO_x and NO_2 in the polluted layer; in urban pollution conditions during daytime we have considered its value to be about 1.32 (Seinfeld and Pandis, 2006) with an uncertainty of about 10 %. c_τ describes the ratio of the measured NO_x and the originally emitted NO_x; it can be estimated from the NO_x lifetime τ, the wind speed w and the distance of the emission source from the measurements:

$$c_\tau = e^{\frac{t}{\tau}} = e^{\frac{r/w}{\tau}} \quad (7)$$

Here t is the ratio of the radius (r) of the circle and the wind speed (w). Assuming a typical urban plume daytime NO_x lifetime of 5 h (Spicer, 1982) and taking into account the wind speed of the individual days, using Eq. (7), we found c_τ in the range of 1.09–1.18 with uncertainties of about ±0.1 (assuming uncertainties of the lifetime of ±2 h). The total NO_x emissions from within the circles on the different days are shown in Fig. 5. Here the error bars show uncertainties due to missing data at some locations. The total NO_x emissions are found to be similar for the different days in the range 1.2–1.6 × 10^{25} molecules per second.

It should be noted that especially close to strong emission sources, part of the emitted NO might not be quickly converted to NO_2 if the NO mixing ratios locally exceed those of O_3. In such cases complete establishment of the NO_2/NO steady state will eventually take place only after ambient air has mixed with the emitted plume. Thus, since from MAX-DOAS instrument only NO_2 (and not NO) can be detected, the total amount of emitted NO_x might be underestimated close to strong emission sources (see also Ibrahim et al., 2010).

ACPD
11, 19179–19212, 2011

3.2 Up-scaling of emissions for Delhi

The NO_x emissions for the different days (Fig. 5) only reflect the emissions from the encircled areas. In order to make these results comparable within each other and to existing emission inventories, the results have to be up-scaled to the greater Delhi area (bounded in the region indicated in Fig. 1, latitude 28.5° N to 28.77° N and longitude 77.0° E to 77.4° E).

For the up-scaling, we used different proxies for the spatial distribution of the NO_x emissions across the considered area. First, we use the EDGAR emission inventory (version 4.1 for 2005, see Olivier et al., 1998; European commission, 2010), but the spatial resolution of this data set is rather coarse (0.1°). Second, we use data on the population density (obtained from CIESIN, GWPv3, 2010, http://sedac.ciesin.columbia.edu/gpw/global.jsp) with a spatial resolution of 2.5 arc minutes. Third, we apply the distribution of night-time lights measured from satellite during night (NOAA, National geophysical Data Center, 2006, http://www.ngdc.noaa.gov/dmsp/download_radcal.html, Ziskin et al., 2010) with a spatial resolution of 0.5 arc minutes. The respective maps of the different proxies, together with the driving routes of the different days are shown in Fig. 6. For all selected proxies the encircled areas include a substantial fraction of the total Delhi emissions (between 30 and 50 %), but a slightly larger fraction lies still outside of these circles (see Table 1).

Surprisingly, the calculated fractions using the different proxies are found to be quite similar, that gives us confidence of our up-scaling procedure to determine the total emissions of the selected area. Figure 7 summarises the total NO_x emissions using the different proxies; it also includes the corresponding NO_x emissions from the EDGAR data base and study by Gurjar et al. (2004). Compared to these emission estimates, our results are found to be systematically lower indicating that the existing emission inventories might overestimate the true emissions. However, it should be taken into account that our results represent only the conditions during a few measurements, while the other inventories are annual averages.

ACPD
11, 19179–19212, 2011

Table 2 lists the different errors of the derived NO_x emissions. If we assume these errors to be independent, we obtain total uncertainties of about 40 % (see also Ibrahim et al., 2010).

4 Comparison with OMI satellite data

Validation of tropospheric trace gas products from satellite observations is a challenging task for several reasons. First, since satellites measure the vertically integrated tropospheric column density, observations of in-situ surface concentrations can not be directly used for validation purposes. Even if vertical profiles are available from aircraft measurements (e.g. Heland et al., 2002) or balloon soundings (e.g. Sluis et al., 2010), they are often not representative for the whole spatial extent of the satellite ground pixel, which is typically of the order of several hundreds of km^2 or more. Similar arguments hold for observations of the integrated tropospheric column measurements e.g. from MAX-DOAS observations at fixed locations (e.g. Brinksma et al., 2008). Here it is important to note that close to strong emission sources like Megacities, where the validation of tropospheric satellite products is of highest importance, the largest variability and strongest gradients are typically found (Chen et al., 2009).

Information about the spatial variability across a satellite ground pixel can be obtained from mobile measurements like car MAX-DOAS observations (e.g. Volkamer et al., 2006; Wagner et al., 2010), thus we also use the tropospheric NO_2 VCDs obtained during our measurement campaigns in Delhi for the validation of the simultaneous observations of the tropospheric NO_2 VCDs from the OMI instrument (DOMINO product, v1.02, http://www.temis.nl/airpollution/no2.html, see Boersma et al., 2007). We selected OMI satellite observations (Levelt et al. 2002), because the ground pixel sizes are much smaller ($\sim 13 \times 26\,km^2$ in nadir geometry) compared to observations from SCIAMACHY and GOME-2.

Figure 8 shows the comparison of the tropospheric NO_2VCDs on 14 April 2010 from mobile MAX-DOAS and OMI observations. On that day, OMI observes Delhi

ACPD
11, 19179–19212, 2011

at relatively slant viewing angles, and the ground pixel sizes are rather large. Thus, the car MAX-DOAS observations cover only relatively small fractions of the individual ground pixels. Nevertheless, in both data sets similar spatial patterns of NO_2 are observed: highest values of NO_2 are found in the south east, which is consistent with the wind direction on that day (north-westerly wind, see Fig. 4). The car MAX-DOAS observations reveal much finer spatial patterns with stronger spatial gradients, which are not resolved from the OMI data.

The comparison of the tropospheric NO_2 VCDs for 15 April 2010 is shown in Fig. 9. On that day the OMI observations were made almost vertically (nadir geometry), and the satellite pixels are much smaller compared to the observations made on 14 April 2010. Both satellite ground pixels over Delhi are well covered by the car MAX-DOAS observations and similar spatial patterns were observed in both data sets. Again, the car MAX-DOAS observations resolve details on a much finer scale.

Figure 10 shows another validation example from 16 January 2011, when MAX-DOAS observations were carried out along a route from Delhi to Agra (about 225 km). Like in the previous examples the general distribution of the tropospheric NO_2 VCD is found to be similar in both data sets with the highest values at or close to Delhi. An interesting finding is that OMI underestimates the high values over Delhi, but overestimates the low values over rural regions along the route Delhi to Agra.

Figure 11 shows a correlation analysis of all car MAX-DOAS observations (during April 2010 and January 2011) and the coincident OMI satellite data (blue points). Here, all MAX-DOAS observations within an OMI ground pixels were averaged. The error bars indicate the OMI error and the standard deviation of the MAX-DOAS observations, respectively. Using these errors, we performed an orthogonal regression (Cantrell, 2008). A reasonable correlation (coefficient of determination $r^2 = 0.48$) is found, but the slope (0.38) deviates strongly from unity. In contrast, the average of all OMI VCDs to the average of the MAX-DOAS observations is 0.77, and the average of the individual ratios is even 1.07.

ACPD
11, 19179–19212, 2011

In order to investigate the effect of limited spatial sampling in the presence of strong gradients in more detail, a second comparison was made including only observations, for which the car MAX-DOAS observations cover large fractions of the OMI pixels (at least 50 % in east-west direction (defined by the most eastern and most western MAX-DOAS observation within the OMI pixel) like e.g. shown in Fig. 9). Only five measurements fulfilled this criterion. If only these observations are considered, a better correlation (coefficient of determination $r^2 = 0.79$) is obtained, but the results of the orthogonal regression are almost unchanged.

A general finding of this comparison is that high tropospheric NO_2 VCDs are systematically underestimated by OMI, while for low tropospheric NO_2 VCDs the opposite behaviour is found.

The underestimation of high tropospheric NO_2 VCDs by OMI might be partly caused by the shielding of the surface-near NO_2 by aerosols. Here it should, however, be noted that the (effective) cloud fractions for the OMI observations used in our study are found to be very low: 2.3 % on average for all observations; <1.2 % for the sub-set of OMI pixels, which are well covered by the car MAX-DOAS observations. Thus, effects of cloud shielding is considered to be negligible here. Part of the underestimation might also be related to differences between the true (relative) NO_2 height profiles and those assumed in the satellite retrieval. If e.g. the assumed profiles contain a smaller fraction close to the surface compared to the true profiles, the respective tropospheric AMFs overestimate the true tropospheric AMFs, and consequently, the retrieved tropospheric NO_2 VCDs underestimate the true tropospheric NO_2 VCDs. If in contrast the fraction close to the surface in the assumed profile is larger than in the true profile, the retrieved tropospheric NO_2 VCDs overestimate the true tropospheric NO_2 VCDs.

These dependencies can qualitatively explain the observed comparison results, since the NO_2 profile data for the OMI retrieval are taken from an atmospheric model (TM4) with a rather coarse spatial resolution (2° latitude and 3° longitude) (Boersma et al., 2007). In contrast, the true atmospheric profiles will most probably change on much finer spatial scales from urban to rural regions. Accordingly, the trace gas fraction close

ACPD
11, 19179–19212, 2011

to the surface in the model profiles probably underestimates the true fraction close to strong emission sources, but probably overestimates it in more rural regions.

5 Conclusions

Car MAX-DOAS observations were performed in the greater Delhi area during April 2010 and January 2011. The aims of the measurements were first the determination of the total NO_x emissions of the greater Delhi area and second the validation of satellite observations.

The total NO_x emissions were derived from observations along closed circles around the city. Since the MAX-DOAS observations encircled only part of the entire Delhi area, we had to up-scale our results. For that purpose we used three different proxies: the spatial distribution of (a) the NO_x emissions from the EDGAR data base, (b) population density, and (c) light intensity observed from satellite during night. Although the first two proxies have rather coarse spatial resolution, the up-scaled results using the three proxies agree well (within 20 %). Two additional corrections were applied to account for the partitioning of NO and NO_2 and for the limited lifetime of NO_x (leading to destruction of part of the emitted NO_x between the locations of the emission source and the observation). The overall uncertainty of our emission estimate taking into account measurement uncertainties and uncertainties of the various assumptions is about 40 %. From four measured circles around Delhi (three during April 2010 and one in January 2011) an average value of 3.74×10^{25} molec/s was derived. The results from the four days were found to agree within ±30 %.

Our NO_x emission estimate is slightly lower than NO_x emissions from the EDGAR data base (v4.1) (4.94×10^{25} molec s^{-1}) and substantially lower than from a recent study by Gurjar et al. (2004) (6.42×10^{25} molec s^{-1}). However, no exact agreement should be expected, because our measurements represent short periods during two months of two contrast seasons (winter and summer), whereas the values from emission inventories are annual averages.

ACPD
11, 19179–19212, 2011

We also used the results from the MAX-DOAS observations for the validation of tropospheric NO_2 VCDs obtained from the OMI instrument on the AURA satellite. We chose OMI observations because of its relatively small pixel sizes. In general, similar spatial patterns are found in both data sets, but with a much finer spatial resolution in the car MAX-DOAS data. The comparison of absolute values show overall a fair agreement. However, the OMI observations tend to underestimate high tropospheric NO_2 VCDs while they tend to overestimate low tropospheric NO_2 VCDs. Most probably, the systematic differences between OMI and car MAX-DOAS observations are caused by differences between the true vertical NO_2 profiles and those assumed in the data retrieval algorithm.

The service charges for this open access publication have been covered by the Max Planck Society.

Acknowledgements. The research leading to these results has received funding from the European Union's Seventh Framework Programme FP/2007-2011 within the project "MEGAPOLI", grant agreement no. 212520. The authors are thankful for the help and support received from Ravi Singh, Vice-Chancellor and Sunil Mishra, Dean Research, Sharda University to carry out Car MAX-DOAS observations in Delhi and sponsoring visit of MS and AC to the Max Planck Institute for Chemistry. We acknowledge the free use of tropospheric NO_2 column data from the OMI sensor from www.temis.nl. We acknowledge European Commission, Joint Research Centre (JRC)/Netherlands Environmental Assessment Agency (PBL) Emission Database for Global Atmospheric Research (EDGAR), release version 4.1. http://edgar.jrc.ec.europa.eu, 2010. Population density Grids are taken from the Center for International Earth Science Information Network (CIESIN), Columbia University; and Centro Internacional de Agricultura Tropical (CIAT). 2005. Gridded Population of the World Version 3 (GPWv3): Population Density Grids. Palisades, NY: Socioeconomic Data and Applications Center (SEDAC), Columbia University. Available at http://sedac.ciesin.columbia.edu/gpw. ECMWF operational analysis data provided by ECMWF. For Radiance Night-time lights, we acknowledge Daniel Ziskin. Data processing by NOAA's National Geophysical Data Center. DMSP data collected by the US Air Force Weather Agency.

ACPD

11, 19179–19212, 2011

References

Balk, D. and Yetman, G.: The global distribution of population: evaluating the gains in resolution refinement, New York: Center for International Earth Science Information Network (CIESIN), Columbia University, http://sedac.ciesin.columbia.edu/gpw, 2005, 2004.

Bobrowski, N., Hönninger, G., Galle, B., and Platt, U.: Detection of bromine monoxide in a volcanic plume, Nature, 423, 273–276, 2003.

Boersma, K. F., Eskes, H. J., Veefkind, J. P., Brinksma, E. J., van der A, R. J., Sneep, M., van den Oord, G. H. J., Levelt, P. F., Stammes, P., Gleason, J. F., and Bucsela, E. J.: Near-real time retrieval of tropospheric NO_2 from OMI, Atmos. Chem. Phys., 7, 2103–2118, doi:10.5194/acp-7-2103-2007, 2007.

Bogumil, K., Orphal, J., Homann, T., Voigt, S., Spietz, P., Fleischmann, O.C., Vogel, A., Hartmann, M., Kromminga, H., Bovensmann, H., Frerik, J., and Burrows, J. P.: Measurements of Molecular Absorption Spectra with the SCIAMACHY Pre-Flight Model: Instrument Characterization and Reference Data for Atmospheric Remote-Sensing in the 230–2380 nm Region, J. Photochem. Photobiol. A., 157, 167–184, 2003.

Brinksma, E. J., Pinardi, G., Volten, H., Braak, R., Richter, A., Schönhardt, A., Van Roozendael, M., Fayt, C., Hermans, C., Dirksen, R. J., Vlemmix, T., Berkhout, A. J. C., Swart, D. P. J., Ötjen, H., Wittrock, F., Wagner, T., Ibrahim, O. W., de Leeuw, G., Moerman, M., Curier, R. L., Celarier, E. A., Knap, W. H., Veefkind, J. P., Eskes, H. J., Allaart, M., Rothe, R., Piters, A. J. M., and Levelt, P. F.: The 2005 and 2006 DANDELIONS NO_2 and Aerosol Validation Campaigns, J. Geophys. Res., 113, D16S46, doi:10.1029/2007JD008808, 2008.

Cantrell, C. A.: Technical Note: Review of methods for linear least-squares fitting of data and application to atmospheric chemistry problems, Atmos. Chem. Phys., 8, 5477–5487, doi:10.5194/acp-8-5477-2008, 2008.

Chen, D., Zhou, B., Beirle, S., Chen, L. M., and Wagner, T.: Tropospheric NO_2 column densities deduced from zenith-sky DOAS measurements in Shanghai, China, and their application to satellite validation, Atmos. Chem. Phys., 9, 3641–3662, doi:10.5194/acp-9-3641-2009, 2009.

Deutschmann, T., Beirle, S., Frieß, U., Grzegorski, M., Kern, C., Kritten, L., Platt, U., Pukite, J., Wagner, T., Werner, B., and Pfeilsticker, K.: The Monte Carlo Atmospheric Radiative Transfer Model McArtim: Introduction and Validation of Jacobians and 3D Features, J. Quant. Spectr. Rad. Transf., 112, 1119–1137, doi:10.1016/j.jqsrt.2010.12.009, 2011.

ACPD
11, 19179–19212, 2011

Elsayed, N. M.: Toxicity of nitrogen dioxide: an introduction, Toxicology, 89(3), 161–74, 1994.
European Commission, Joint Research Centre (JRC)/Netherlands Environmental Assessment Agency (PBL).: Emission Database for Global Atmospheric Research (EDGAR), release version 4.1. http://edgar.jrc.ec.europa.eu, 2010
Fayt, C. and Van Roozendael, M.: WinDOAS 2.1 Software User Manual, (http://www.oma.be/BIRA-IASB/Molecules/BrO/WinDOAS-SUM-210b.pdf), 2001.
Gautam, R., Hsu, N. C., Kafatos, M., and Tsay, S.-C.: Influences of winter haze on fog/low cloud over the Indo-Gangetic plains, J. Geophys. Res., 112, D05207, doi:10.1029/2005JD007036, 2007.
Goyal, S. K., Ghatge, S. V., Nema, P., and Tamhane, S. M.: Understanding urban vehicular pollution problem vis-à-vis ambient air quality – case study of a megacity (Delhi, India), Environ. Monit. Assess., 119, 557–569, doi:10.1007/s10661-005-9043-2, 2006.
Greenblatt, G. D., Orlando, J. J., Burkholder, J. B., and Ravishankara, A. R.: Absorption measurements of oxygen between 330 and 1140 nm, J. Geophys. Res., 95, 18577–18582, 1990.
Gurjar, B. R., Aardenne, J. A. van, Lelieveld, J., and Mohan, M.: Emission estimates and trends (1990–2000) for megacity Delhi and implications, Atmos. Environ., 38, 5663–5681, 2004.
Heland, J., Schlager, H., Richter, A., and Burrows, J. P.: First comparison of tropospheric NO_2 column densities retrieved from GOME measurements and in situ aircraft profile measurements, Geophys. Res. Lett., 29(20), 1983, doi:10.1029/2002GL015528, 2002.
Hermans, C., Vandaele, A. C., Carleer, M., Fally, S., Colin, R., Jenouvrier, A., Coquart, B., and Mérienne, M.-F., Absorption Cross-Sections of Atmospheric Constituents, NO_2, O_2, and H_2O, Environ. Sci. & Pollut. Res., 6, 151–158, 1999.
Hönninger G. and Platt U.: Observations of BrO and its vertical distribution during surface ozone depletion at Alert, Atmos. Environ., 36, 2481–2490, 2002.
Ibrahim, O., Shaiganfar, R., Sinreich, R., Stein, T., Platt, U., and Wagner, T.: Car MAX-DOAS measurements around entire cities: quantification of NO_x emissions from the cities of Mannheim and Ludwigshafen (Germany), Atmos. Meas. Tech., 3, 709–721, doi:10.5194/amt-3-709-2010, 2010.
Jacob, D. J.: Introduction to Atmospheric Chemistry, Princeton University Press, 1999.
Johansson, M., Galle, B., Yu, T., Tang, L., Chen, D., Li, H., Li, J. X., and Zhang, Y.: Quantification of total emission of air pollutants from Beijing using mobile mini-DOAS, Atmos. Environ., 42, 6926–6933, 2008.
Johansson, M., Rivera, C., de Foy, B., Lei, W., Song, J., Zhang, Y., Galle, B., and Molina, L.:

ACPD
11, 19179–19212, 2011

Mobile mini-DOAS measurement of the outflow of NO_2 and HCHO from Mexico City, Atmos. Chem. Phys., 9, 5647–5653, doi:10.5194/acp-9-5647-2009, 2009.
Kraus, S.: DOASIS, A Framework Design for DOAS, PhD-thesis, University of Mannheim, available at: (http://hci.iwr.uni-heidelberg.de/publications/dip/2006/Kraus_PhD2006.pdf), 2006.
Kurucz, R. L., Furenlid, I., Brault, J., and Testerman, L.: Solar flux atlas from 296 nm to 1300 nm, National Solar Observatory Atlas No. 1, Office of University publisher, Harvard University, Cambridge, 1984.
Lal, S.: Trace gases over the Indian region, Indian J. Radio Space, 36, 556–579, 2007.
Levelt, P.F. and Noordhoek, R.: OMI Algorithm Theoretical Basis Document Volume I: OMI Instrument, Level 0-1b Processor, Calibration & Operations, Tech. Rep. ATBD-OMI-01, Version 1.1, 2002.
Olivier, J. G. J., Bouwman, A. F., Van der Hoek, K. W., and Berdowski, J. J. M.: Global air emission inventories for anthropogenic sources of NO_x, NH_3 and N_2O in 1990, Environ. Pollut., 102, 135–148., 1998.
Platt, U. and Stutz, J.: Differential Optical Absorption Spectroscopy, Principles and Applications, Springer, Berlin, 2008.
Ramanathan, V. and Ramana, M. V.: Persistent, Widespread and Strongly Absorbing Haze over the Himalayan Foothills and the Indo-Ganges Plains, Pure and Applied Geophysics, 162, 1609–1626, doi:10.1007/s00024-005-2685-8, 2005.
Ramanathan, V., Chung, C., Kim, D., Bettge, T., Buja, L., Kiehl, J. T., Washington, W. M., Fu, Q., Sikka, D. R., and Wild, M.: Atmospheric brown clouds: Impacts on South Asian climate and hydrological cycle, Proc. Natl. Acad. Sci. USA, 102, 5326-5333, 2005.
Ravishankara, R., Liu, S., Platt, U., Bates, T., Bey, I., Carslaw, K., Chipperfield, M., Douglass, A., Fahey, D., Feingold, G., Fuzzi, S., Gettleman, A., Granier, C., Hauglustine, D., Mari, C., O'Neill, A., Parrish, D., Quinn, P., Randel, W., Rosenlof, K., Shepherd, T. and Simon, P.: Climate Chemistry Interactions, Report from the joint SPARC/IGAC workshop, 3-5 April 2003, Giens, France, http://www.atmosp.physics.utoronto.ca/SPARC/RelatedPublications/IGAC_SPARC_FINAL.pdf, 2004.
Rivera, C., Sosa, G., Wöhrnschimmel, H., de Foy, B., Johansson, M., and Galle, B.: Tula industrial complex (Mexico) emissions of SO_2 and NO_2 during the MCMA 2006 field campaign using a mobile mini-DOAS system, Atmos. Chem. Phys., 9, 6351–6361, doi:10.5194/acp-9-6351-2009, 2009.
Rothman, L.S., Jacquemart, D., Barbe, A., Benner, D. C., Birk, M., Brown, L.R., Carleer, M.R.,

ACPD
11, 19179–19212, 2011

Chackerian Jr., C., Chance, K., Coudert, L.H., Dana, V., Devi, V.M., Flaud, J.-M. , Gamache, R.R., Goldman, A., Hartmann, J.-M., Jucks, K.W., Maki, A.G., Mandin, J.-Y., Massie, S.T., Orphal, J., Perrin, A., Rinsland, C.P., Smith, M.A.H., Tennyson, J., Tolchenov, R.N., Toth, R.A., Vander Auwera, J., Varanasi, P., and Wagner, G.: The HITRAN 2004 molecular spectroscopic database, J. Quant. Spectrosc. Ra., 96 139–204, 2005.

Seinfeld, J. H. and Pandis, S. N.: From air pollution to climate change, Atmospheric Chemistry and Physics, John Wiley & Sons, New York 2nd Edn, 2006.

Sheel, V., Lal, S., Richter, A., and Burrows, J. P.: Comparison of satellite observed tropospheric NO_2 over India with model simulations, Atmos. Environ., 44, 3314–3321, doi:10.1016/j.atmosenv.2010.05.043, 2010.

Singh, R. P., Dey, S., Tripathi, S. N., Tare, V., and Holben, B.: Variability of aerosol parameters over Kanpur, northern India, J. Geophys. Res., 109, D23206, doi:10.1029/2004JD004966, 2004.

Singh, R. P., Prasad, A. K., Chauhan, S. S. S., and Singh, S.: Impact of growing urbanization and air pollution on the regional climate over India, International Association for Urban Climate Newsletter, Issue No. 14, December 2005, 5–10, 2005.

Sluis, W. W., Allaart, M. A. F., Piters, A. J. M., and Gast, L. F. L.: The development of a nitrogen dioxide sonde, Atmos. Meas. Tech., 3, 1753–1762, doi:10.5194/amt-3-1753-2010, 2010.

Spicer, C. W.: Nitrogen Oxide Reactions in the Urban Plume of Boston. Science, 215, 1095–1097, 1982.

Vandaele, A. C., Hermans, C., Simon, P.C., Roozendael, M., Guilmot, J. M., Carleer, M. and Colin, R.: Fourier transform measurement of NO_2 absorption cross-section in the visible range at room temperature, J. Atmos. Chem., 25(3), 289–305, 1996.

Van Roozendael, M., Fayt, C., Post, P., Hermans, C., and Lambert, J.-C.: Retrieval of BrO and NO_2 from UV-Visible Observations, in: Sounding the troposphere from space: a new era for atmospheric chemistry, edited by: Borell, P., Borrell, P. M., Burrows, J. P., and Platt, U., Springer, Heidelberg, ISBN 3-540-40873-8, 2004.

Volkamer, R., Spietz, P. and Burrows, J. and Platt, U.: High-resolution absorption cross-section of glyoxal in the UV-vis and IR spectral ranges, J. Photoch. Photobio. A, 172, 35—46, 2005.

Volkamer, R., Kurosu, T. P., Chance, K., Li, Z., Zhang, Y., Brauers, T., and Wahner, A.: Spatial Variability of Glyoxal, HCHO and NO_2 during PRD-2006: Comparison of mobile Mini-MAX-DOAS and OMI satellite data in the Pearl River Delta, China, Eos Trans. AGU, 87(52), Fall Meet. Suppl., Abstract, A31B-0897, 2006.

ACPD
11, 19179–19212, 2011

Wagner, T., Dix, B., Friedeburg, C. V., Frieß, U., Sanghavi, S., Sinreich, R., and Platt, U.: MAX-DOAS O_4 measurements – a new technique to derive information on atmospheric aerosols. (I) Principles and information content, J. Geophys. Res., 109, D22205, doi:10.1029/2004JD004904, 2004.

Wagner, T., Ibrahim, O., Shaiganfar, R., and Platt, U.: Mobile MAX-DOAS observations of tropospheric trace gases, Atmos. Meas. Tech., 3, 129–140, doi:10.5194/amt-3-129-2010, 2010.

Wagner, T., Beirle, S., Brauers, T., Deutschmann, T., Frieß, U., Hak, C., Halla, J. D., Heue, K. P., Junkermann, W., Li, X., Platt, U., and Pundt-Gruber, I.: Inversion of tropospheric profiles of aerosol extinction and HCHO and NO_2 mixing ratios from MAX-DOAS observations in Milano during the summer of 2003 and comparison with independent data sets, Atmos. Meas. Tech. Discuss., 4, 3891–3964, doi:10.5194/amtd-4-3891-2011, 2011.

Wittrock, F., Oetjen, H., Richter, A., Fietkau, S., Medeke, T., Rozanov, A., and Burrows, J. P.: MAX-DOAS measurements of atmospheric trace gases in Ny-Ålesund - Radiative transfer studies and their application, Atmos. Chem. Phys., 4, 955–966, doi:10.5194/acp-4-955-2004, 2004.

World Health Organization, Health Aspects of Air. Pollution with Particulate Matter, Ozone and Nitrogen Dioxide. Report on a WHO Working Group, 13–15 January 2003, Bonn, Germany, 2003.

Ziskin, D., Kimberly, B., Feng, C.H., Tilottama, G., and Chris, E.: Methods Used For the 2006 Radiance Lights, Proceedings of the 30th Asia-Pacific Advanced Network Meeting, 131–142, http://www.ngdc.noaa.gov/dmsp/download_radcal.html, 2010.

ACPD
11, 19179–19212, 2011

Table 1. Fraction of the EDGAR NO_x emissions, population, and light within the surrounded areas for the different days.

day	fraction based on EDGAR emission density	fraction based on population density	fraction based on night-time lights
13 April 2010	43 %	45 %	42 %
14 April 2010	49 %	42 %	43 %
15 April 2010	42 %	35 %	35 %
15 January 2011	36 %	33 %	33 %

ACPD
11, 19179–19212, 2011

Table 2. Uncertainties of the different steps of the emission estimate.

Error of	due to	see Sect.	13 April 2010	14 April 2010	15 April 2010	15 January 2011
SCD	Spectral analysis	2.3			15 %	
VCD	Geometric Approx.	2.5			20 %	
NO_2 flux	Wind fields	3.1			18 %	
	Measurement gaps	3.1	21 %	8 %	9 %	1 %
NO_x flux	c_L	3.1			10 %	
	c_τ	3.1			10 %	
New Delhi emissions	Upscaling	3.2			10 %	
Total	Squareroot of quadratic sum	3.2	41 %	36 %	36 %	35 %

ACPD
11, 19179–19212, 2011

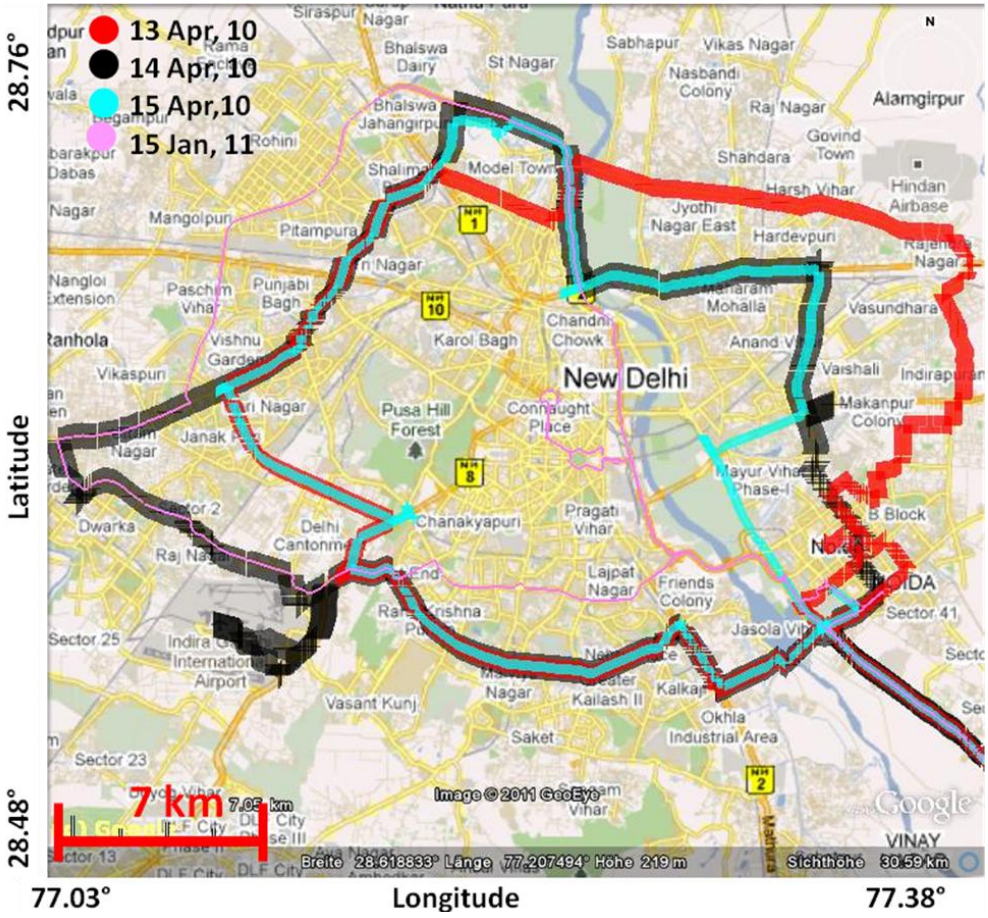

Fig. 1. Different driving routes around Delhi.

ACPD
11, 19179–19212, 2011

Estimation of NO_x emissions from Delhi

R. Shaiganfar et al.

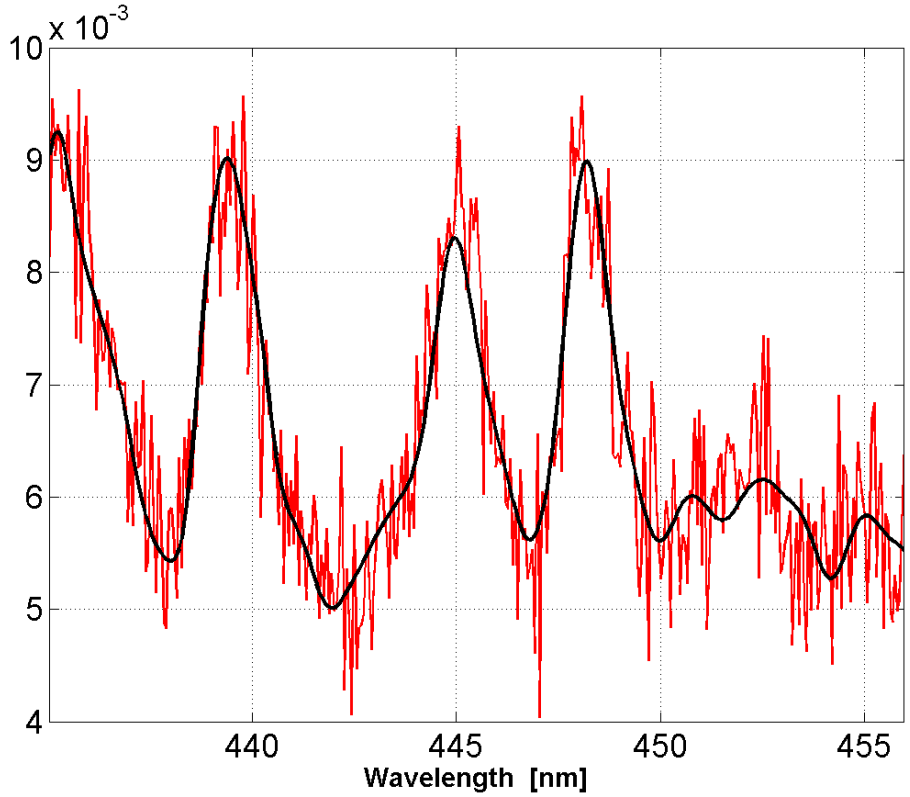

Fig. 2. Typical result of the DOAS fit. Shown are the NO_2 cross-section scaled by the respective absorption of the measured spectrum (black). The red curve shows in addition the fit residual.

ACPD
11, 19179–19212, 2011

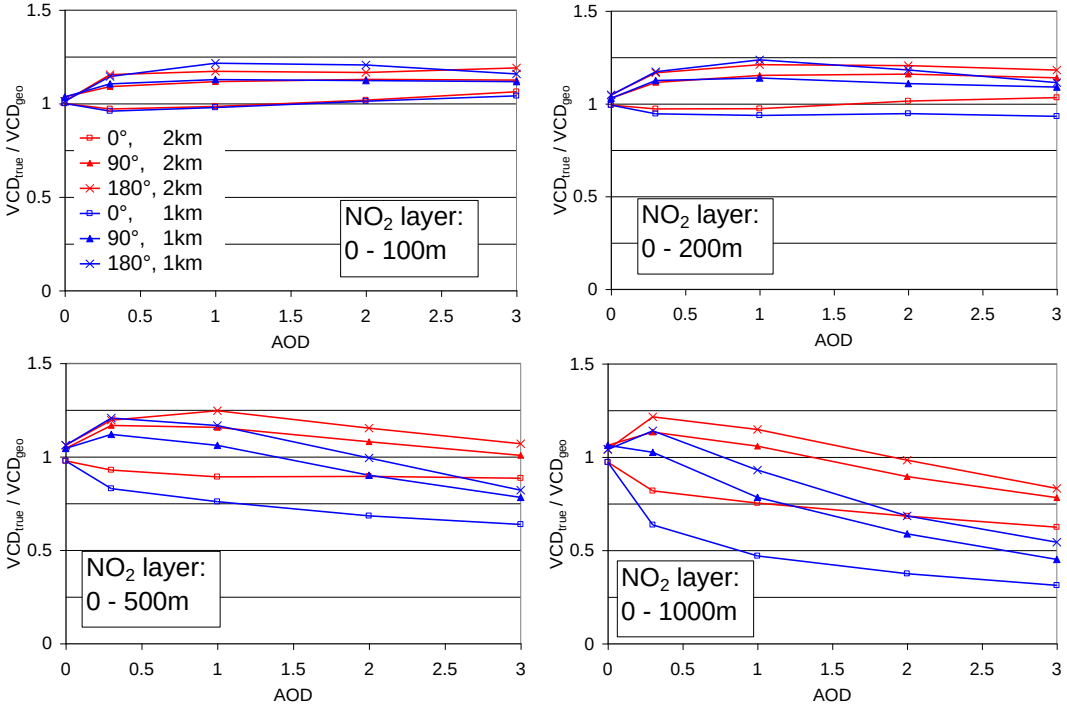

Fig. 3. Relative deviation of the true tropospheric VCDs (derived from radiative transfer simulations) from the geometric VCD for different trace gas layer heights, aerosol optical depth, aerosol layer heights and relative azimuth angles (i.e. the difference of the azimuth angles of the sun and the viewing direction at the telescope). Calculations are performed for an elevation angle of 22°; the results for an elevation angle of 30° (not shown) are similar.

ACPD
11, 19179–19212, 2011

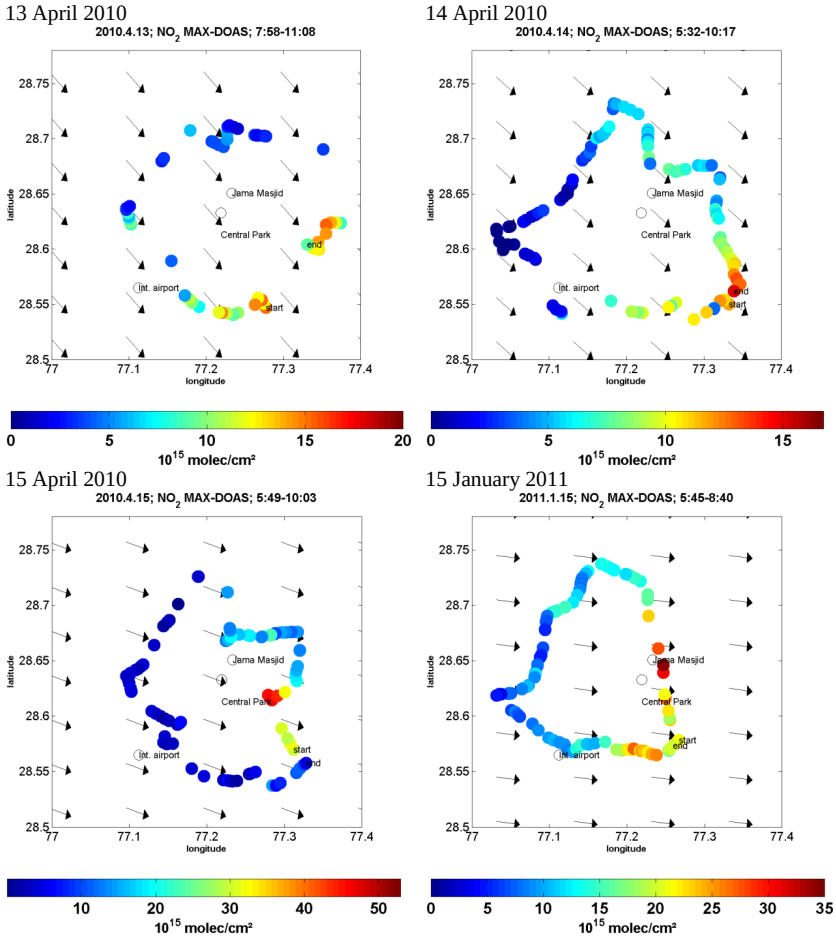

Fig. 4. Tropospheric NO_2 VCDs derived from car MAX-DOAS observations around Delhi on different days. The arrows indicate the average wind direction.

ACPD
11, 19179–19212, 2011

Estimation of NO_x emissions from Delhi

R. Shaiganfar et al.

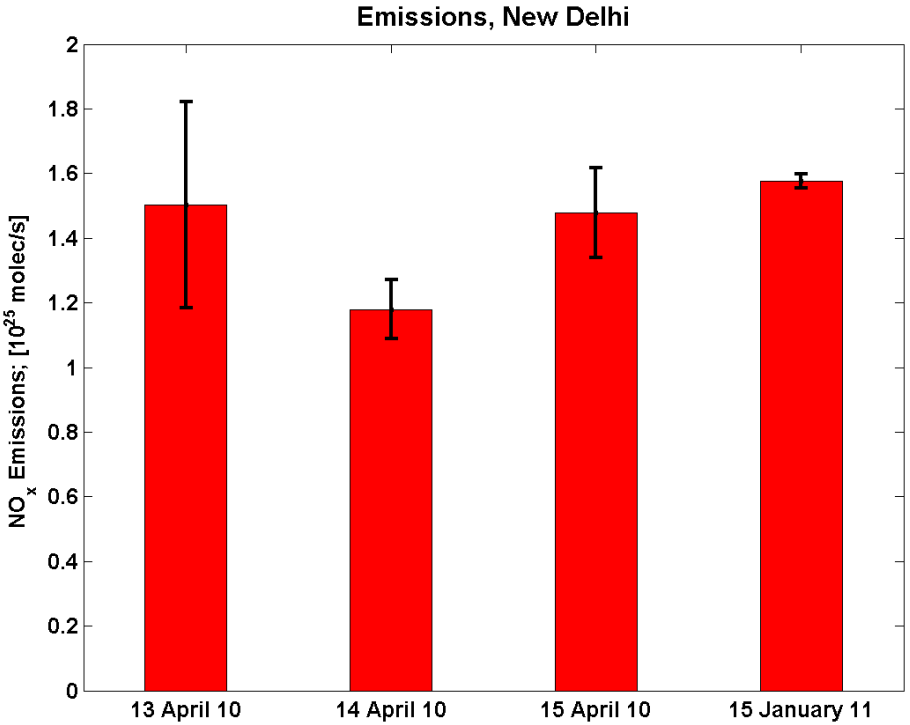

Fig. 5. NO_x emissions obtained from the car MAX-DOAS measurements for the surrounded areas. The error bars indicate uncertainties due to measurement gaps along the driving routes.

ACPD
11, 19179–19212, 2011

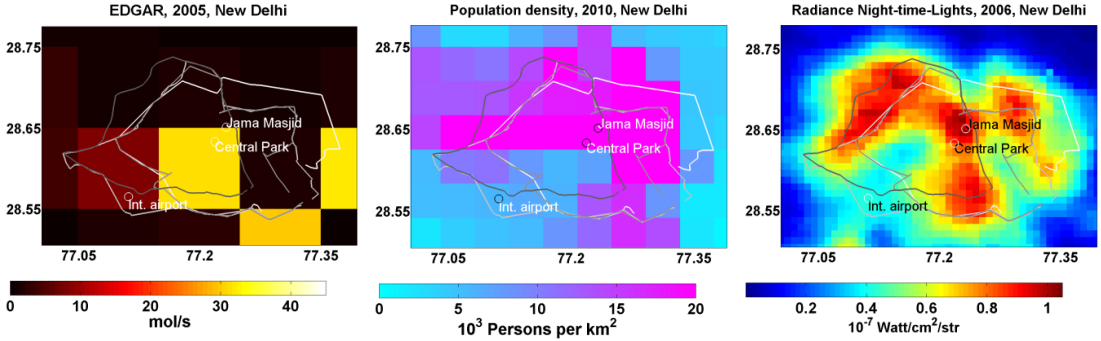

Fig. 6. Spatial distribution of the NO_x emissions from the EDGAR data base (left), of the population density (center), and the night-time lights (right) for the selected Delhi area (see Fig. 1). Also shown are the driving routes for the different days.

ACPD
11, 19179–19212, 2011

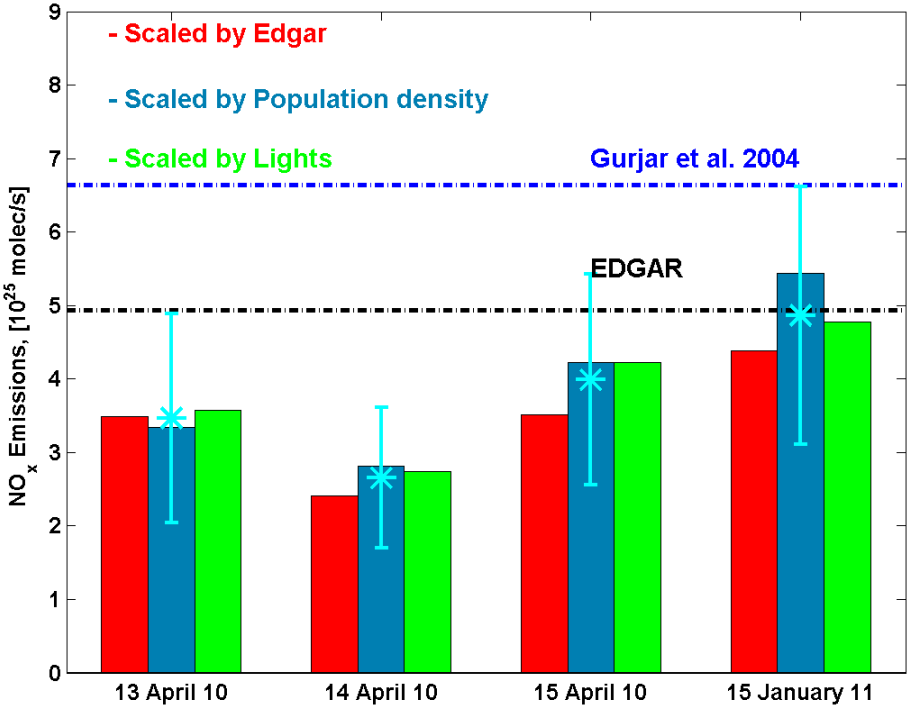

Fig. 7. Comparison of the up-scaled NO_x emissions from the car MAX-DOAS measurements (using different proxies) and existing emission estimates. The cyan points show the mean emission estimate for each day with the respective total error, as explained in Table 2.

ACPD
11, 19179–19212, 2011

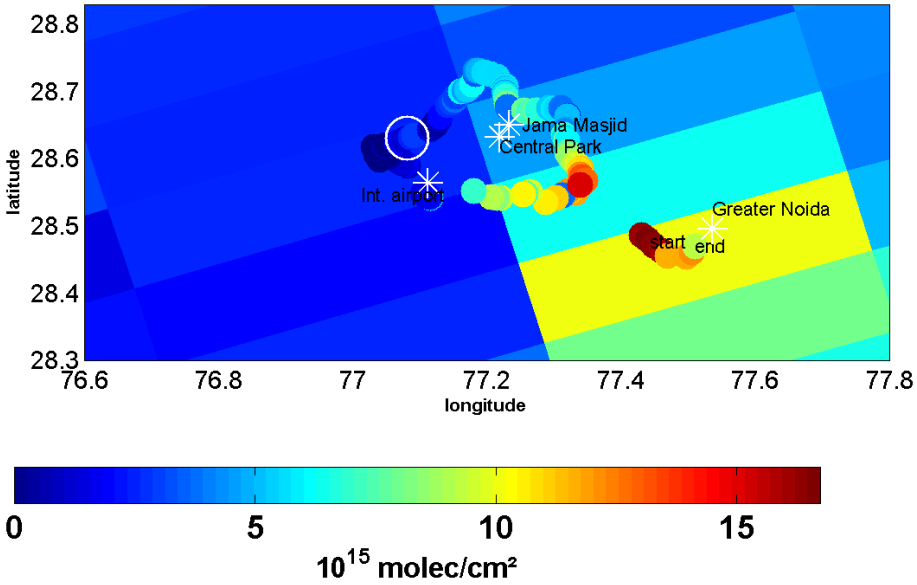

Fig. 8. Comparison of the tropospheric NO_2 VCDs on 14 April 2010 measured from OMI and car MAX-DOAS. MAX-DOAS observations were carried out between 05:20 and 10:57 UT; OMI overpass was at 07:50 UT. The large circle indicates MAX-DOAS observations during the OMI overpass.

ACPD
11, 19179–19212, 2011

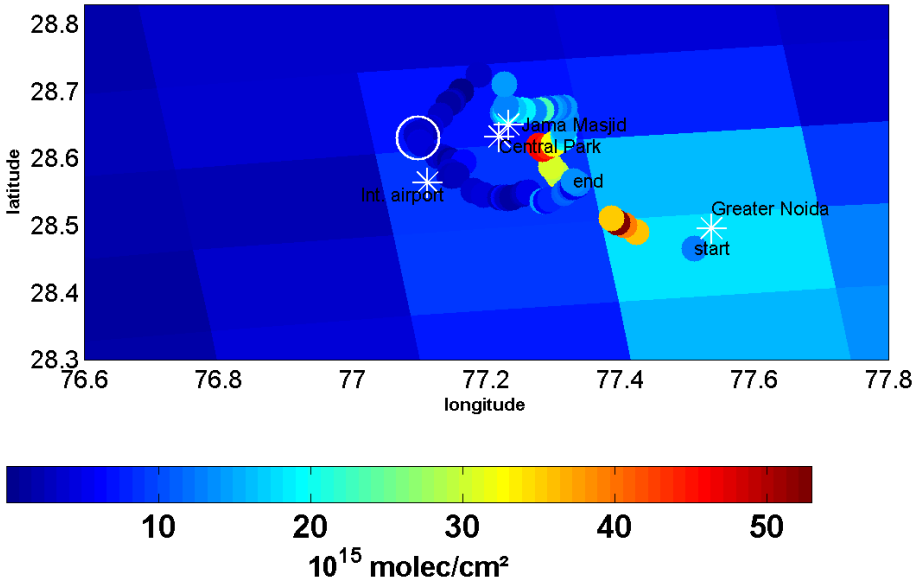

Fig. 9. Comparison of the tropospheric NO_2 VCDs on 15 April 2010 measured from OMI and car MAX-DOAS. MAX-DOAS observations were carried out between 05:05 and 10:06 UT; OMI overpass was at 08:33 UT. The large circle indicates MAX-DOAS observations during the OMI overpass.

ACPD
11, 19179–19212, 2011

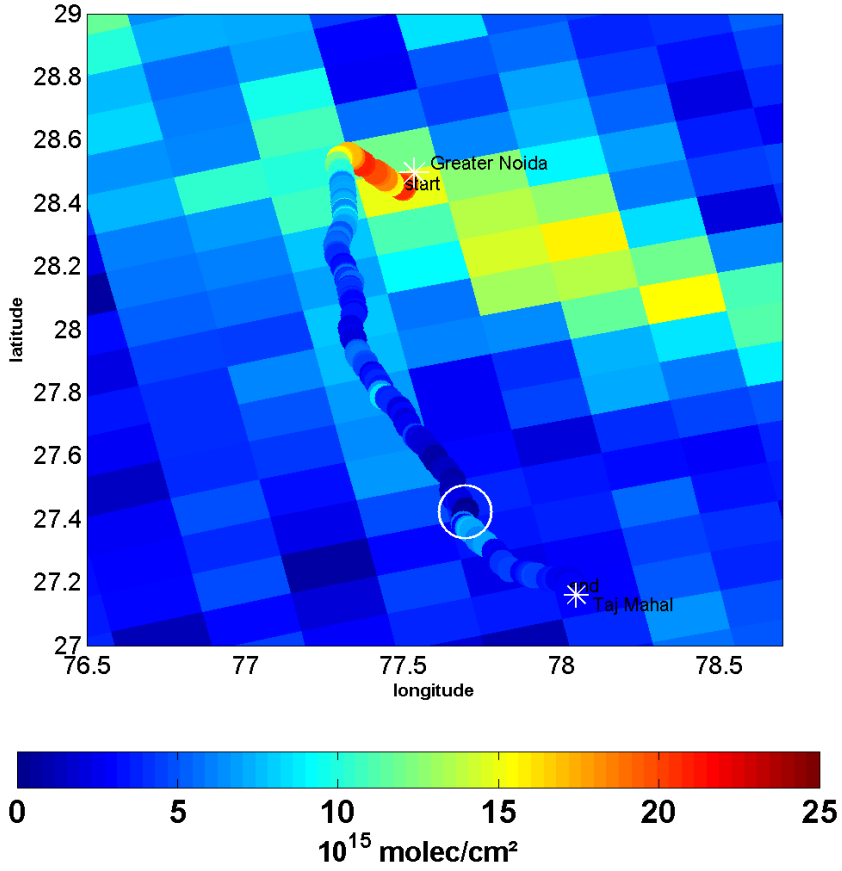

Fig. 10. Comparison of the tropospheric NO_2 VCDs on 16 January 2011 measured from OMI and car MAX-DOAS from New Delhi to Agra (Taj Mahal). MAX-DOAS observations were carried out between 04:33 and 09:05 UT; OMI overpass was at 08:06 UT. The large circle indicates MAX-DOAS observations during the OMI overpass.

ACPD
11, 19179–19212, 2011

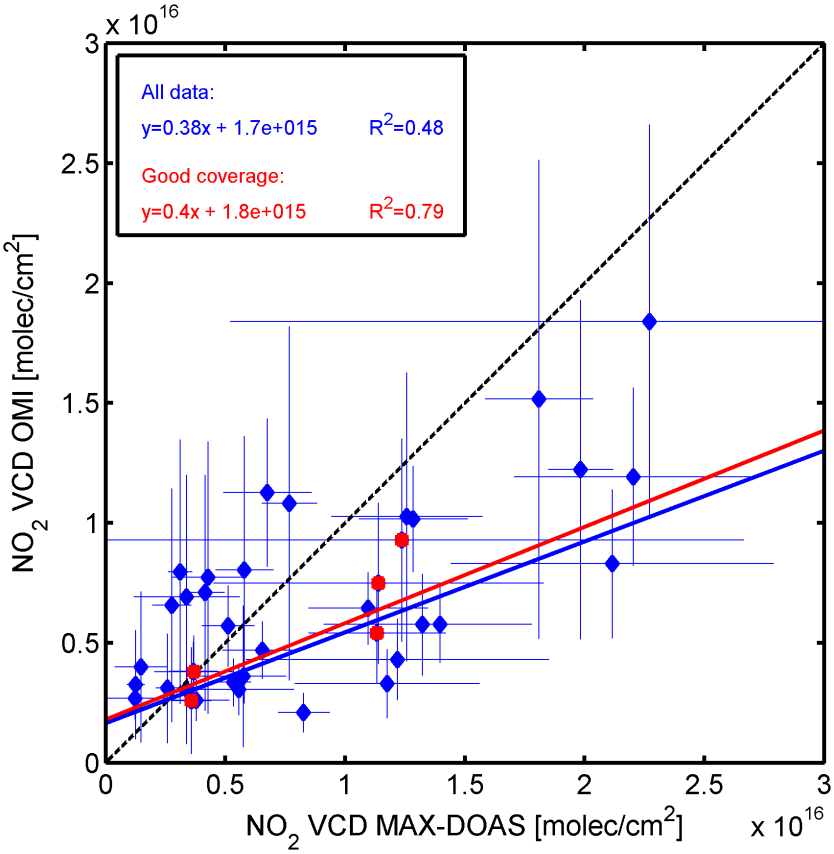

Fig. 11. Correlation analysis of OMI and car MAX-DOAS observations of the tropospheric NO_2 VCD during April 2010 and January 2011. Blue dots represent all coincident measurements; red dots represent measurements where the OMI ground pixels were mostly covered (at least 50 % in east-west dimension) by the car MAX-DOAS measurements (like in Fig. 9).

ACPD
11, 19179–19212, 2011